Received: 27 April 2022 | Revised: 15 August 2022 | Accepted: 31 August 2022

DOI: 10.1002/er.8755

RESEARCH ARTICLE

INTERNATIONAL JOURNAL OF ENERGY RESEARCH WILEY

# Model-based diagnosis of proton-exchange membrane fuel cell cathode catalyst layer microstructure degradation

**Hamed Heidari**[1] | **Qadir Esmaili**[2] | **Ali Akbar Ranjbar**[1]

[1]School of Mechanical Engineering, Babol University of Technology, Babol, Iran

[2]Faculty of Engineering, Amol University of Special Modern Technologies, Amol, Iran

**Correspondence**
Qadir Esmaili, Faculty of Engineering, Amol University of Special Modern Technologies, Amol, Iran.
Email: q.esmaili@ausmt.ac.ir

## Summary

It is of vital importance to utilize diagnostic tools that are capable of quickly identifying faulty conditions during cell operation. Electrochemical impedance spectroscopy (EIS) is a popular technique for monitoring proton-exchange membrane fuel cell (PEMFC) performance and physics-based models are a sophisticated tool for predicting cell behavior and interpreting the data achieved by EIS. In this study, a transient, one-dimensional, two-phase model for PEMFC membrane electrode assembly (MEA) was developed. By coding in MATLAB, the system of equations was solved and EIS spectra were obtained over the frequency range of 0.1 Hz to 100 kHz. The effects of Pt loss and ionomer distribution on EIS spectrum were investigated. The results indicate that the low-frequency intercept of the impedance spectrum with the real axis, also known as the low-frequency resistance (LFR), is an ideal indicator of Pt degradation and if not mitigated in the early stages, Pt degradation can significantly deteriorate cell electrochemical performance (up to 27% increase in LFR for the cases studied). The impact of heterogeneous ionomer distribution in cathode catalyst layer (CCL) on the high-frequency portion of the impedance spectrum, also known as the "straight line" in the literature, is investigated. The results show that the length and the slope of the straight line are great indicators of ionomer degradation as the slope of the straight line deviated up to 16° from the ideal 45° (in case of a uniform distribution of ionomer in CCL) and the length of the straight line decreased about 44% for the cases studied.

## Highlights

- A transient, one-dimensional, two-phase model of proton-exchange membrane fuel cell suitable for diagnostic applications is developed.
- Effects of cathode catalyst layer microstructure degradation on cell electrochemical impedance spectrum are investigated.
- The low-frequency resistance is an ideal indicator of Pt degradation.
- The shape of the high-frequency portion of the impedance spectrum could be utilized for ionomer degradation monitoring.

KEYWORDS

cathode catalyst layer degradation, diagnosis and monitoring, electrochemical impedance spectroscopy, one-dimensional model, proton exchange membrane fuel cell

  

## 1 | INTRODUCTION

Due to the disadvantages of fossil fuels, interest and financial investments in the field of renewable energy have significantly increased.[1] Meanwhile, PEMFC technology has attracted substantial attention because of its advantages of high efficiency, low emission, and fast response.[2] However, there are still barriers to the commercialization of PEM fuel cells such as manufacturing costs and durability.[3] Degradation can escalate, if not mitigated in early stages,[4] which highlights the importance of diagnostic and monitoring tools that can quickly identify faulty conditions during cell operation.[5]

One of the most popular methods for diagnosing and monitoring PEMFC performance is electrochemical impedance spectroscopy (EIS).[6] EIS involves applying a low-amplitude harmonic stimulus signal to the cell and measuring the impedance response of the cell. Since the applied stimulus signal has a small amplitude, the cell operation is not disturbed. EIS is capable of providing comprehensive information on a broad range of phenomena regarding cell performance such as charge transfer properties, reaction mechanisms, and electrode health status. Zhang et al[7] carried out a review of the common PEMFC electrochemical diagnostic methods and concluded that the EIS provides the most diagnostic dimensions and least system disturbance. However, EIS analysis could be quite challenging due to ambiguities in interpretation.[8] To facilitate the analysis of the EIS data, two major modeling strategies have been presented in the literature.

The most common approach for modeling the impedance of PEMFC is the equivalent circuit (EC) model.[9,10] This strategy involves simulating physical and chemical processes as a network of resistors and capacitors called equivalent electrical circuit. Equivalent values for resistors and capacitors are obtained by fitting the impedance of the system with experimental data. EC models are simple to implement and have low computational costs; however, they are not capable of predicting cell's impedance behavior and lack proper physical interpretation.[5]

Over the last few years, physics-based models have been widely used to interpret EIS data. In this strategy, PEMFC behavior during EIS tests is simulated based on the governing equations of the physical and chemical phenomena that occur in the cell; thus, proper physical interpretation can be attained from EIS spectra. In particular, agglomerate models can provide valuable insights into catalyst layer microstructure by taking charge and mass transfer through the cathode catalyst layer (CCL) into account.[11] Based on the modeling approach, physics-based models are classified into two categories of analytical and computational.

Several authors[12,13] have developed analytical models to simulate the impedance behavior of PEMFC. Analytical models are computationally efficient and capable of providing valuable insights into the fundamental physics of the cell. However, to obtain the solution of analytical models, simplifying assumptions have to be made that compromises the generality of the model or oversimplifies the underlying physics of the cell.

Therefore, it is necessary to develop computational models that incorporate more complex phenomena without compromising the accuracy of the solution or comprehensiveness of the model. Recently, multi-dimensional computational fluid dynamics (CFD) simulations have attained more popularity due to accessibility of PEMFC modeling packages in commercial software such as COMSOL and Ansys Fluent. Baricci et al[14] simulated EIS for the first time in 3D and used CFD to investigate oxygen transport in a low platinum PEMFC. However, water management and two-phase flow were not incorporated in their study. Hence, the simulation results deviated from experimental data in operating conditions where liquid water effects were significant. Xie et al[15] developed a three-dimensional multi-phase model of PEMFC including an improved agglomerate submodel of CCL with realistic agglomerate size. The improved agglomerate model was capable of considering the effects of platinum loading on cell performance more accurately than traditional agglomerate models. Falcao et al[16] proposed a single-phase one-dimensional model, and a three-dimensional model in single-phase and two-phase modes for PEMFC. Comparison of these models with experimental data indicates that in the single-phase mode, there is negligible difference between the results of the one-dimensional and three-dimensional models. While the CPU time for the one-dimensional model was about 5 min, it took about 24 h for the three-dimensional model to be computed. Both models overestimate the cell performance in single-phase mode, but the two-phase model is in good agreement with the experimental data. Multi-dimensional CFD models are very demanding in terms of computational resources and their convergence could be challenging.[17] This highlights the necessity of computational one-dimensional models that are capable of adjusting the balance between accuracy and computational cost which is crucial for monitoring and diagnostic applications.[18,19]

Gerteisen[20] developed a one-dimensional model of CCL and investigated the effects of heterogeneous distribution of catalyst layer parameters such as protonic conductivity and volumetric double layer capacity on the impedance spectrum of CCL. Lee et al[21] numerically studied the EIS data of flooding and dehydration degradations using an EC model coupled with a one-

dimensional physics-based model. Their coupled model was capable of predicting cell performance under various operating conditions.

Operating conditions like startup-shutdown, idling, and dynamic loading trigger degradation mechanisms such as carbon corrosion, generation of free radicals, and mechanical degradation leading to detachment of Pt particles, redistribution, and chemical degradation of ionomer.[22] CCL durability has a major impact on the lifetime of PEMFC[23] and microstructure changes in CCL due to degradation can disturb cell performance.[24] Therefore, extensive study of the CCL microstructure is crucial for improving PEMFC durability.

In the present study, a one-dimensional, two-phase model for membrane electrode assembly (MEA) of PEMFC is developed. The CCL is simulated using a modified agglomerate model capable of accurately predicting the effects of microstructure changes of CCL on PEMFC performance. The model incorporates the effects of liquid water and the transient processes of CCL are accurately simulated. The computational domain is divided into three subdomains and the equations of each subdomain are solved separately. This methodology can decrease the system's number of degrees of freedom which results in further computational savings.[25] The model's accuracy and computational efficiency make it a novel and effective in-situ tool for degradation and performance monitoring.

Conducting experiments has proven to be challenging due to the small thickness of CCL and analytical expressions for CCL impedance must be re-derived for every specific distribution of ionomer.[26] Very few numerical studies in the literature have investigated ionomer degradation in MEAs with heterogeneous ionomer distribution in CCL and its impacts on the cell impedance spectrum. Therefore, the objective of this study is to shed light on the interactions between CCL microstructure degradation and EIS data and to provide a reference to facilitate the interpretation of EIS data as an electrode health assessment tool.


FIGURE 1 Computational domain

TABLE 1 Governing equations

| Description | Equations | Components |
|---|---|---|
| Electric potential | $c_{dl}\frac{\partial \varphi_e}{\partial t}=\frac{\partial}{\partial x}\left(\sigma_e\frac{\partial \varphi_e}{\partial x}\right)+S_{\varphi_e}$ | GDL, CL |
| Ionic potential | $c_{dl}\frac{\partial \varphi_i}{\partial t}=\frac{\partial}{\partial x}\left(\sigma_i\frac{\partial \varphi_i}{\partial x}\right)+S_{\varphi_i}$ | CL, membrane |
| Gas species | $\frac{\partial}{\partial t}\left(\epsilon^{eff}c_i\right)=\frac{\partial}{\partial x}\left(D_i^{eff}\frac{\partial c_i}{\partial x}\right)+S_i$ | GDL, CL |
| Liquid pressure | $\frac{\partial}{\partial t}(\varepsilon\rho_L s)=\frac{\partial}{\partial x}\left[\frac{\rho_L K_w(s)}{\mu_L}\frac{\partial P_c}{\partial s}\frac{\partial s}{\partial x}\right]+S_{H_2O}^l$ | GDL, CL |
| Water content | $-\frac{\rho_{mb}}{EW}\frac{\partial \lambda}{\partial t}=\frac{\partial N_{w,mb}}{\partial x}+S_\lambda$ | CL, membrane |

TABLE 2 Source terms of governing equations

| Source terms | Expressions |
|---|---|
| Electric potential and ionic potential (A m$^{-3}$) | $S_{\varphi_i}=-S_{\varphi_e}=-j$ |
| Oxygen (kg m$^{-3}$ s$^{-1}$) | $S_{o_2}=-\frac{j}{nF}$ |
| Liquid water (kg m$^{-3}$ s$^{-1}$) | $S_{H_2O}^l\begin{cases}S_{H_2O}^{phase}+\left(\frac{j}{2F}-S_\lambda\right)M_{H_2O}\ in\ CL\\ S_{H_2O}^{phase}\ in\ other\ zones\end{cases}$ |
| Water evaporation and condensation (kg m$^{-3}$ s$^{-1}$) | $S_{H_2O}^{phase}=\begin{cases}K_{cond}\Delta P\frac{\varepsilon(1-s)x_{wv}M_{H_2O}}{RT}\ if\ \Delta P=\left(Px_{wv}-P_{wv}^{sat}\right)\geq 0\\ K_{cond}\Delta P\varepsilon\rho\ if\ \Delta P=\left(Px_{wv}-P_{wv}^{sat}\right)<0\end{cases}$ |
| Water content (mol m$^{-3}$ s$^{-1}$) | $S_\lambda=\begin{cases}\zeta_{a\frac{\rho^{Naf}}{EW}\left(\lambda^{equal}-\lambda\right)}\ in\ CL\\ 0\ in\ other\ zones\end{cases}$ |

## 2 | MODEL DESCRIPTION

### 2.1 | Governing equations

Figure 1 illustrates the one-dimensional computational domain composed of three parts including: CCL, gas diffusion layer (GDL), and PEM. In this model, Faraday's law is applied to describe the relation between electric current and reactants consumption in electrochemical reactions. Electron and proton transport is governed by Ohm's law and Butler-Volmer equation describes the relation between current and potential. Gaseous reactant transport is described by Fick's diffusion law and water behavior in membrane is represented by empirical correlations.

Fluid flow is assumed to be two-phase and fully saturated and the main mechanism of liquid motion in porous media is capillary force. Other assumptions applied to the model are:

- All gases behave as ideal gases.
- Incompressible and laminar fluid flow.
- Phase transition happens instantly and its effects are insignificant.
- Due to low velocity and pressure difference, the momentum of gas species is neglected.

Tables 1 and 2 show the governing equations of the model and their source terms, respectively. Transport

**TABLE 3** Transport properties and empirical correlations

| Parameters | Expressions |
|---|---|
| Gas diffusivities ($m^{-2}\ s^{-1}$) | $D_i^{eff} = D_i(1-s)^{1.5}$ |
| Capillary pressure (Pa) | $p_c = \frac{\sigma cos\theta_c}{\sqrt{\frac{k}{\varepsilon}}} J(s)$ |
| Leverett function | $J(s) = \begin{cases} 1.417(1-s) - 2.120(1-s)^2 + 1.263(1-s)^3 \ for\ \theta < 90^\circ \\ 1.417s - 2.120s^2 + 1.263s^3 \ for\ \theta > 90^\circ \end{cases}$ |
| Equilibrium membrane water content | $\lambda^{equil} = \begin{cases} 1.41 + 11.3a_{H_2O} - 18.8{a_{H_2O}}^2 + 16.2{a_{H_2O}}^3\ 0 \le a_{H_2O} \le 1 \\ 10.1 + 2.94(a_{H_2O} - 1)\ 1 < a_{H_2O} \le 3 \\ 16\ 3 < a_{H_2O} \end{cases}$ |
| Electro osmotic drag coefficient | $n_d = \frac{2.5}{22}\lambda$ |
| Water activity | $a_{H_2O} = x_{H_2O}\frac{P_v}{P_{sat}} + 2s$ |
| Membrane protonic conductivity (S cm−1) | $\left(0.020634 + 0.01052\lambda - 1.0125 \times 10^{-4}\lambda^2\right) \times \frac{6248}{R} \times \left(\frac{1}{303} - \frac{1}{T}\right)$ |
| Bruggeman's correlation for CCL Protonic conductivity (S cm−1) | $\sigma_i^{CCL} = \sigma_i \varepsilon_{im}^{1.5}$ |
| Flux of water in membrane (mol $m^{-3}$ $s^{-1}$) | $N_{w,mb} = -\frac{\rho_{mb}}{EW} D_w \frac{\partial \lambda}{\partial x} + n_d \frac{i_{fc}}{F}$ |
| Diffusion coefficient of liquid water in membrane ($m^{-2}\ s^{-1}$) | $D_w = \begin{cases} 3.1 \times 10^{-7}\lambda\left(e^{0.28\lambda} - 1\right)e^{-\frac{2436}{T}} for\ 0 < \lambda < 3 \\ 4.17 \times 10^{-8}\lambda\left(161e^{-\lambda} + 1\right)e^{-\frac{2436}{T}} for\ 3 \le \lambda < 17 \end{cases}$ |

**TABLE 4** Conservation laws used for coupling subdomains

| | x = **0** | **GDL/CL** | **CL/MEM** | x = L |
|---|---|---|---|---|
| $C_{o_2}$ | $C_{o_2} = c_{o_2}^{ref}$ | $N_{o_2}^{GDL} = N_{o_2}^{CL}$ | $N_{o_2}^{membrane} = 0$ | N/A |
| $\varphi_i$ | N/A | $i_p^{cl} = 0$ | $i_p^{cl} = i_p^{membrane}$ | $\varphi_i = 0$ |
| $\varphi_s$ | $i_e^{GDL} = I_{cell}$ | $i_e^{GDL} = i_e^{CCL}$ | $i_e^{membrane} = 0$ | N/A |
| S | $S = 0$ | $N_{lq}^{GDL} = N_{lq}^{CL}$ | $N_{lq}^{Mem} = 0$ | N/A |
| $\lambda$ | N/A | $N_w^{GDL} = 0$ | $N_w^{CCL} = N_w^{membrane}$ | $N_w = N_{w,anode}^{eq}$ |

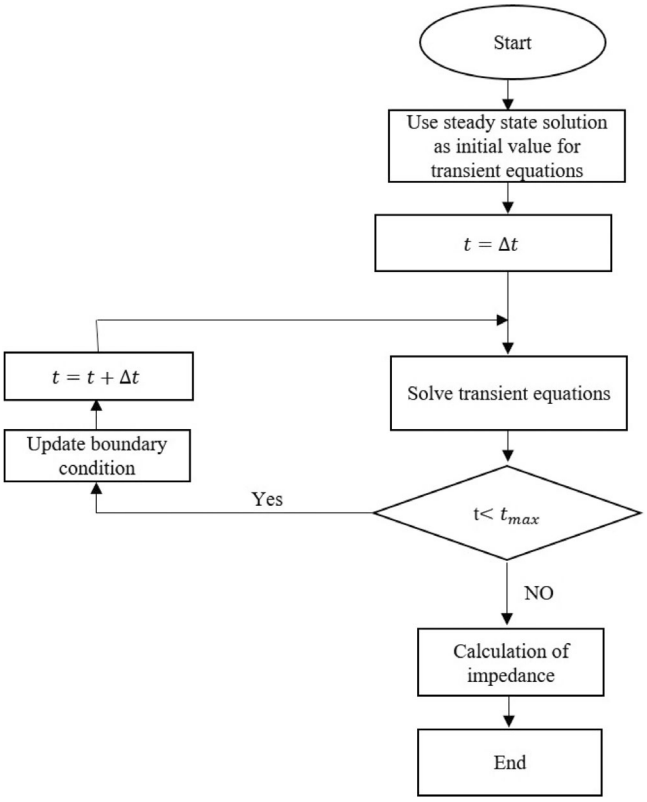


FIGURE 2 Flowchart of the iterative scheme

properties and empirical correlations used in the model are listed in Table 3.

## 2.2 | Agglomerate model of CCL

The CCL submodel is based on the modified agglomerate model developed by Xie et al.[15] The modified agglomerate model is capable of predicting the effects of microstructure changes of CCL on cell performance more accurately than traditional agglomerate models due to considering a more reasonable agglomerate size. In the following, the formulation of the CCL submodel is briefly presented.

Volume fraction of each phase of CCL is calculated as:

$$\varepsilon_{Pt/c} = \frac{m_{Pt}}{\delta_{CL}}\left[\frac{1}{\rho_{Pt}} + \left(\frac{1}{\zeta_{Pt/c}} - 1\right)\frac{1}{\rho_C}\right] \quad (1)$$

$$\varepsilon_{im} = \frac{\zeta_{im/c} m_{Pt}}{\rho_{im}\delta_{CL}}\left(\frac{1}{\zeta_{Pt/c}} - 1\right)\left(1 + \frac{M_{lw}\rho_{im}}{\rho_{lw}EW}\lambda\right) \quad (2)$$

$$\varepsilon_{CL} = 1 - \varepsilon_{Pt/c} - \varepsilon_{im} \quad (3)$$

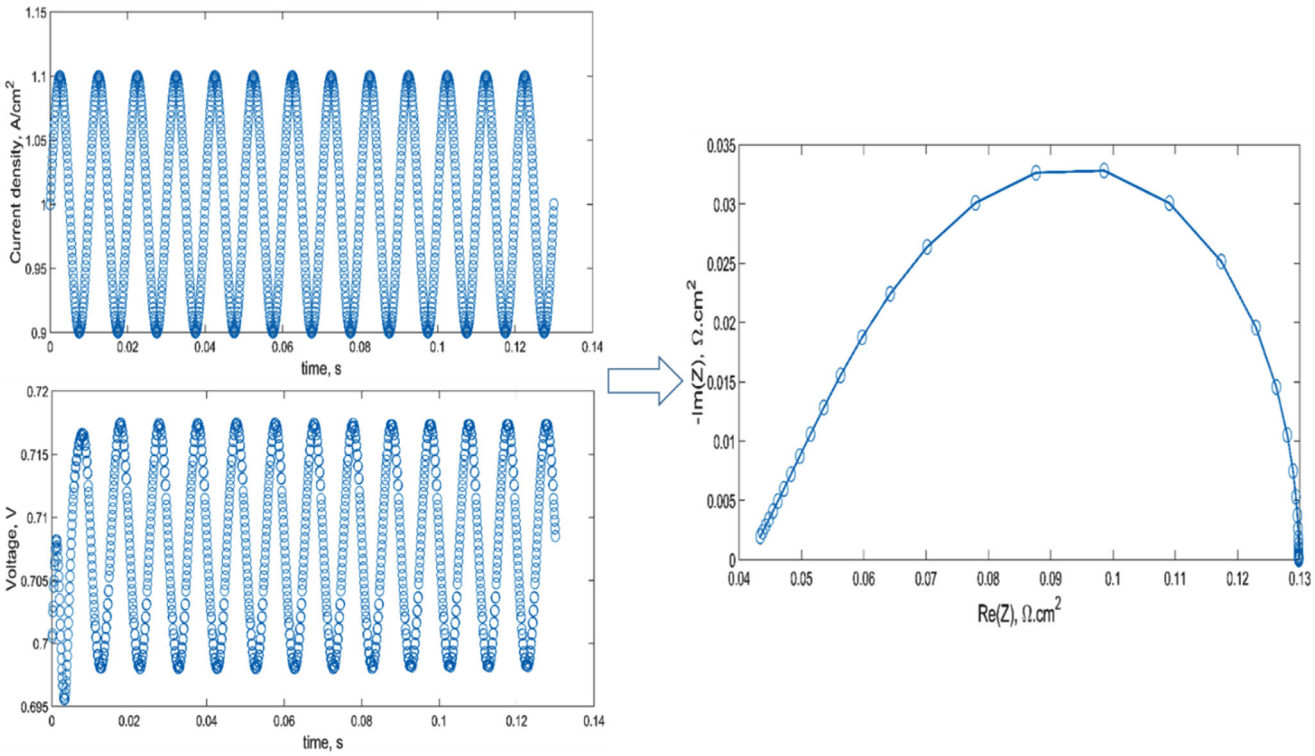


FIGURE 3 Impedance calculation process

The total mass transport resistance of the CCL is obtained by:

$$R_{local} = R_l + R_{int} = (1+k_1)\frac{\delta_w}{D_{O_2,w}} + \left(\frac{A_{im}^{eff}}{A_{pt}^{eff}} + k_2\right)\frac{\delta_{im}}{D_{O_2,im}} + k_3\frac{\delta_{pt}^{eff}}{D_{O_2,pt}^{eff}} \quad (4)$$

$R_{ele}$ is the electrochemical resistance of the CCL:

$$R_{elec} = \frac{4FA_{im}C_{O_2}^{ref}}{k_{ele}} \quad (5)$$

$$k_{elec} = i_{0,c}^{ref}A_{pt}\theta_{T,c}\theta_{pt/im}(1-\theta_{pt/o})\left(\exp\left(-\frac{4F\alpha_c\eta_c}{RT} - \frac{\omega\theta_{pt/o}}{RT}\right) - \exp\left(-\frac{4F\alpha_a\eta_c}{RT}\right)\right) \quad (6)$$

The electrochemical reaction rate is calculated using Butler-Volmer equation:

$$j_c = \frac{4FA_{im}RTC_{O_2}^g/H_{O_2}}{R_{elec}+R_{local}} \quad (7)$$

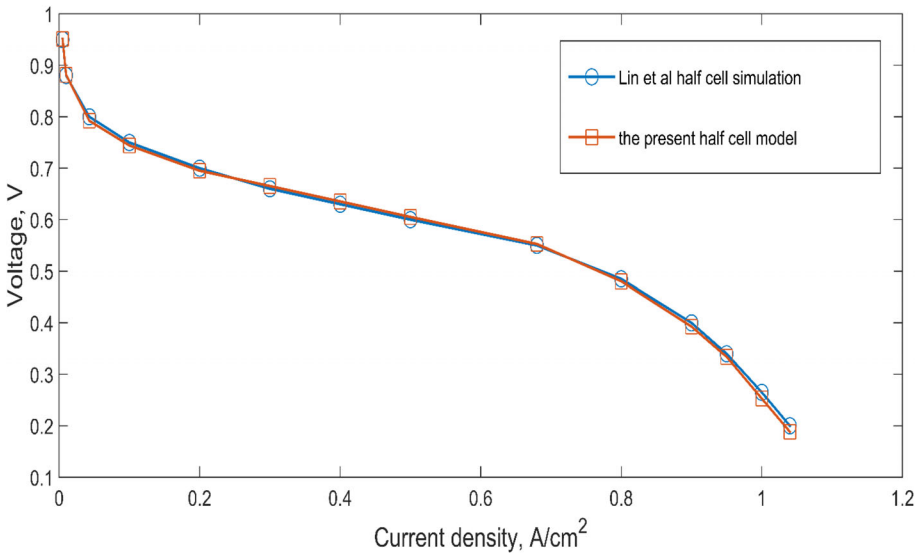


**FIGURE 4** Comparison of polarization curves with Lin et al.[27]

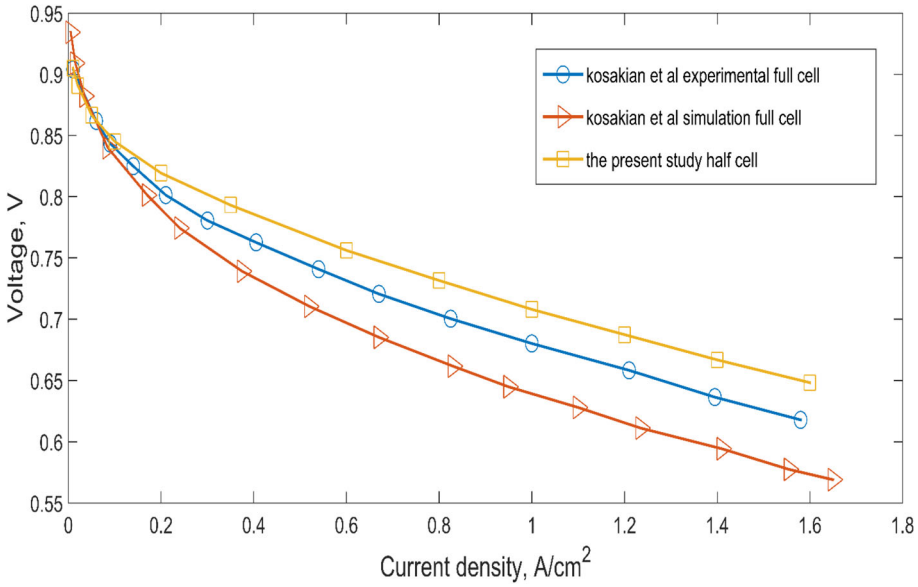


**FIGURE 5** Comparison of the polarization curves with Kosakian et al.[28]

## 2.3 | Numerical procedure

The CCL submodel is incorporated into a transient one-dimensional two-phase model of MEA. To solve the system of equations in steady state, each subdomain is separately solved, and then by implementing conservation laws according to Table 4, subdomains are coupled.

The solution obtained from the steady-state is used as the initial condition to solve the equations in transient state. To ensure that the boundary conditions are being applied in transient state, each time step is broken into

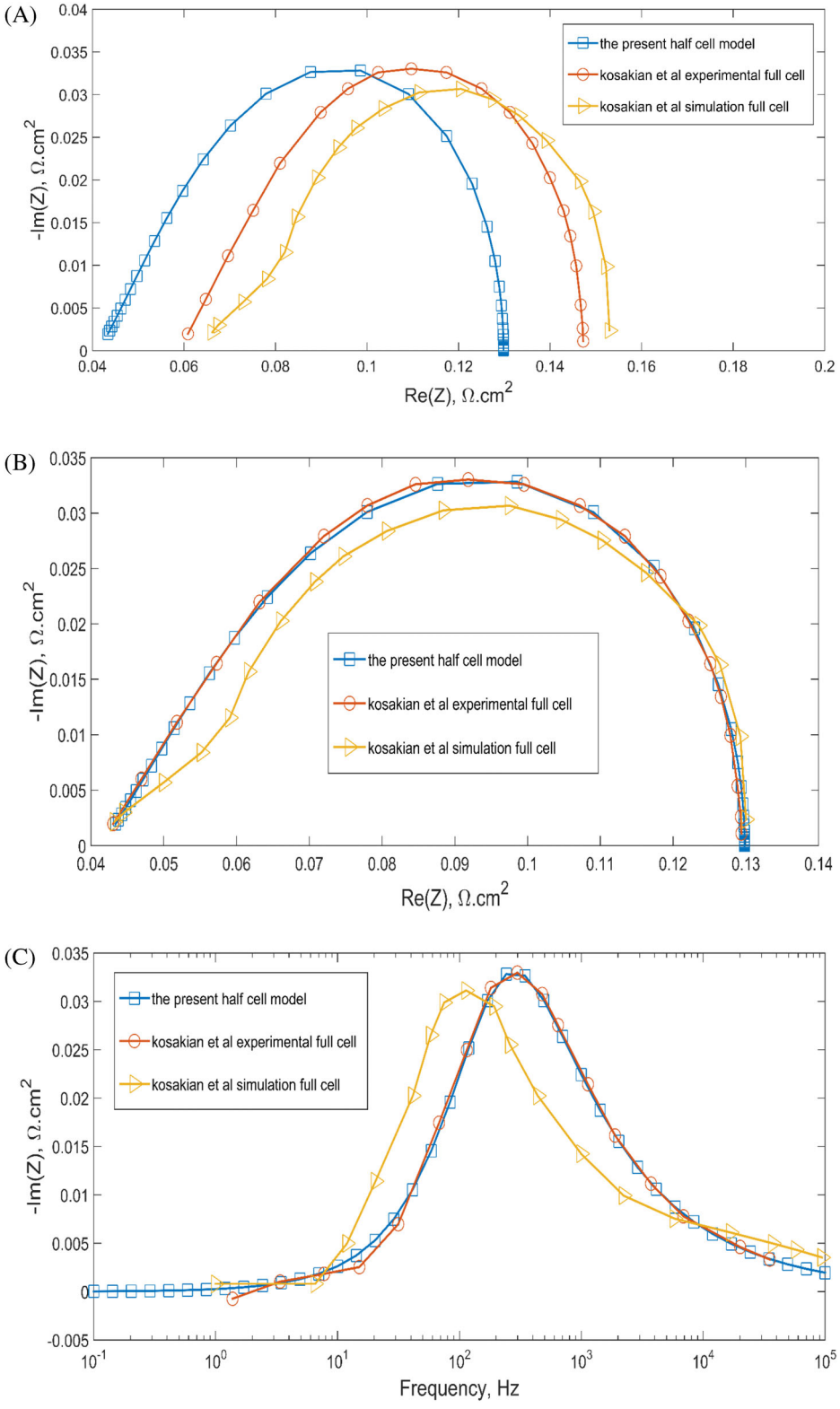


**FIGURE 6** (A) Comparison of the EIS spectra with Kosakian et al[28] under a current density of 1 $A/cm^2$. (B) The impedance spectra of (A) plotted at the same HFR. (C) Comparison of the Bode diagrams with Kosakian et al[28] under a current density of 1 $A/cm^2$. EIS, electrochemical impedance spectroscopy; HFR, high-frequency resistance

much smaller time steps and the solution of each time step is used as initial condition for the next time step. The PDEPE function of MATLAB which is an implementation of the method-of-lines together with a finite-element discretization in space is used to solve the equations in the transient state. Figure 2 shows the flowchart of the algorithm of the numerical solution.

Impedance spectroscopy technique is implemented on the transient solution of the model and the Impedance response of the system is acquired. EIS simulations were

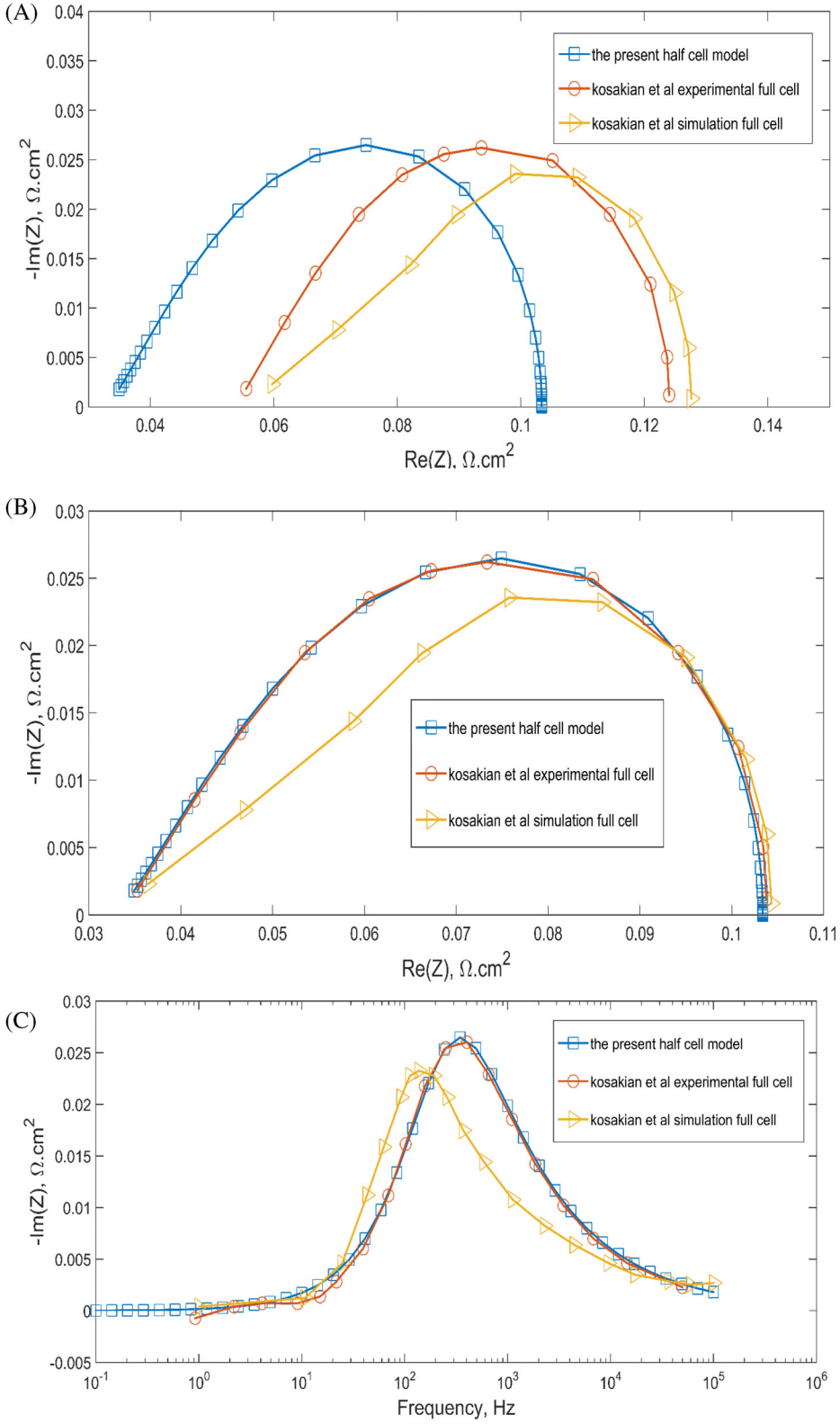


**FIGURE 7** (A) Comparison of the EIS spectra with Kosakian et al[28] under a current density of 1.4 $A/cm^2$. (B) The impedance spectra of (A) plotted at the same HFR. (C) Comparison of the Bode diagrams with Kosakian et al[28] under a current density of 1.4 $A/cm^2$. EIS, electrochemical impedance spectroscopy; HFR, high-frequency resistance

conducted in galvanostatic mode by implementing a harmonic perturbation with an amplitude of 10% of the current. Each spectrum is comprised of 40 points of perturbation frequency in a frequency range of 0.1 Hz to 100 kHz. To ensure the accuracy of EIS simulations especially at higher frequencies, up to 4000 sample frequencies were used for impedance calculation at each perturbation frequency. Figure 3 demonstrates the process of calculating the impedance response of the cell. After utilizing the FFT function of MATLAB to apply Fourier transform and obtain the values of cell voltage and current density in the frequency phase, the Impedance response of the system can be simply calculated as:

$$Z(\omega) = \frac{V(\omega)}{I(\omega)} = \frac{V_0 e^{j(\omega t+\varphi_V)}}{I_0 e^{j(\omega t+\varphi_I)}} \quad (8)$$

## 3 | RESULTS AND DISCUSSION

In the following, first, the consistency of the simulation results and experimental data is investigated, and then the effects of Pt and ionomer degradation on cell performance are simulated.

### 3.1 | Model validation

Model validation has been achieved by comparing two polarization curves and two impedance spectra under different current densities of 1 and 1.4 $A/cm^2$. First, the polarization curve obtained from this work is validated against the half-cell simulation conducted by Lin et al[27] as shown in Figure 4.

Then, the set of parameters and operating conditions used by Kosakian et al[28] are incorporated in the simulations (RH = 50%, $T$ = 80°C, $P$ = 1.5 atm, and pure oxygen in cathode flow) and the shape of the impedance spectra are fitted to the experimental data presented by Kosakian at various current densities. Figure 5 shows that the polarization curves presented by Kosakian and the one predicted by this model show similar trends. It should be noted that the discrepancy in ohmic resistance in polarization curves and impedance spectra is due to the fact that the half-cell model presented in this work does not account for the ohmic losses of the anode electrode and MPL layer of cathode and the same discrepancy between the half cell and full cell performance can be observed in the literature.[29,30]

Figures 6A-C and 7A-C show the impedance spectra under current densities of 1 and 1.4 $A/cm^2$ and their respective Bode diagrams. To facilitate the comparison of trends, the discrepancies in high-frequency resistance (HFR) were subtracted and the impedance spectra presented by Kosakian were shifted along the real axis to the same HFR as the impedance spectra obtained in this study. The shifted impedance spectra are plotted in Figures 6B and 7B. The simulated impedance spectra presented by Kosakian deviate from the experimental data in the high-frequency portion of the impedance spectrum, also known as the "straight line" in the literature. In case of a homogeneous distribution of ionomer, the straight line exhibits a 45° slope as simulated by Kosakian. However, the straight line of the experimental spectra shows a slope steeper than the ideal 45°. Therefore, in

**TABLE 5** Pt loadings and corresponding CCL thicknesses

| Pt loading (mg $cm^{-2}$) | Corresponding thickness of CCL (μm) |
|---|---|
| 0.05 | 1.5 |
| 0.15 | 4.5 |
| 0.25 | 7.5 |
| 0.35 | 10.5 |

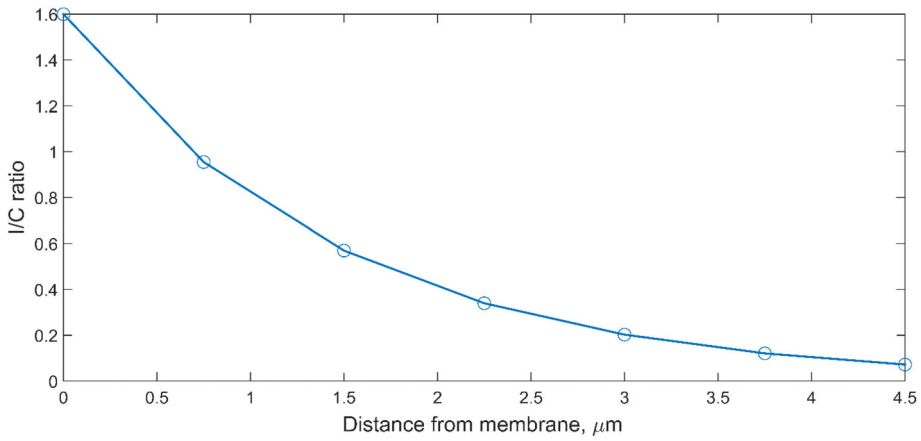


**FIGURE 8** Distribution of ionomer in the CCL. CCL, cathode catalyst layer

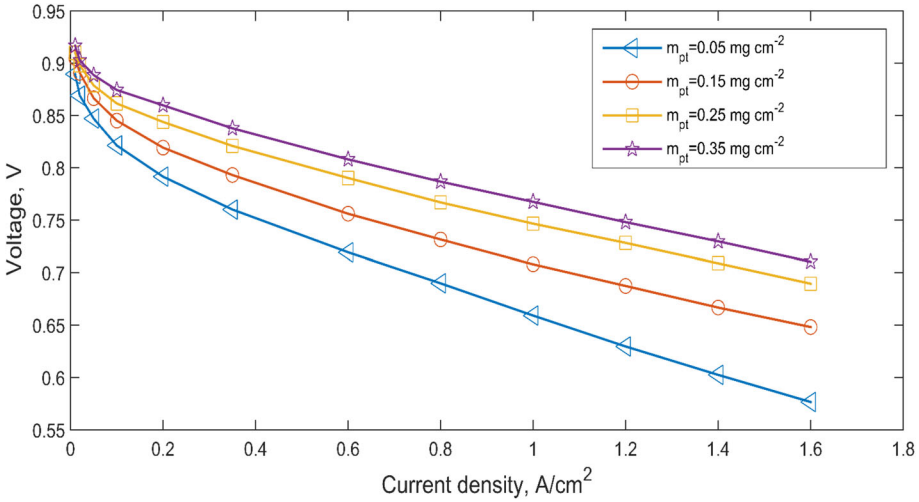


**FIGURE 9** Effect of catalyst loss on polarization curve

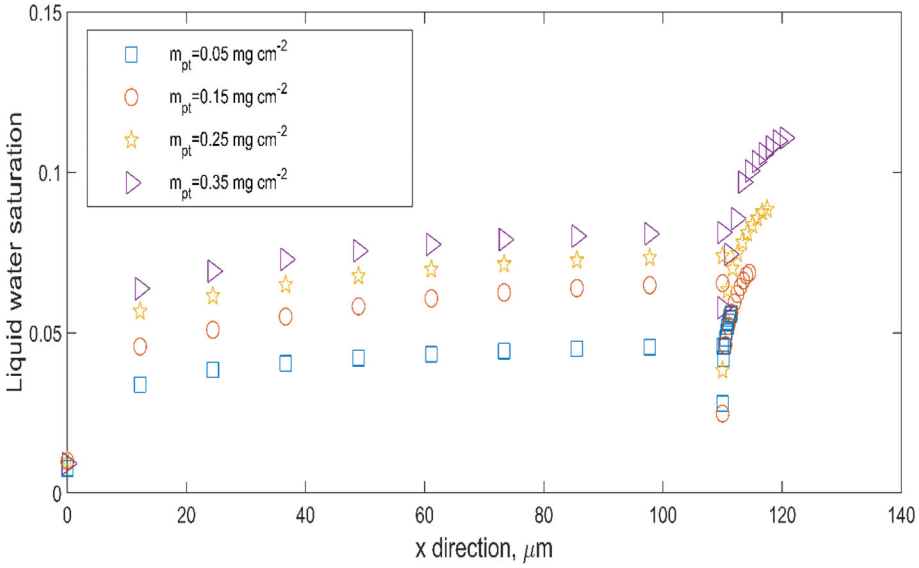


**FIGURE 10** Effect of catalyst loss on liquid water saturation profile across the cathode

this study, a heterogeneous distribution of ionomer in CCL, according to Equation (9) and as shown in Figure 8, was employed to achieve consistency with experimental data in the high-frequency portion of the impedance spectra. This distribution was taken from the literature[31,32] and was obtained by fitting impedance spectra to experimental data. After implementing the ionomer distribution and fitting the impedance spectra to the experimental impedance spectra presented by Kosakian, the values $\beta = 3.1$ and $\zeta^0_{im/c} = 1.6$ were achieved and employed as the base case. The simulated polarization curve and impedance spectra show similar trends as experimental data, confirming the present model's capability to predict PEMFC behavior.

$$\zeta_{im/c} = \zeta^0_{im/c} \exp\left(-\frac{\beta x}{\delta_{CL}}\right) \tag{9}$$

## 3.2 | Degradation of platinum

Platinum is commonly utilized as catalyst in most PEMFCs owing to its high catalytic activity for both oxygen reduction reaction (ORR) and hydrogen oxidation reaction and is the essential parameter affecting cell electrochemical performance. Degradation mechanisms namely carbon corrosion and mechanical degradation lead to detachment of Pt particles and loss of Pt in CCL. In this section, the effects of Pt degradation on cell performance are investigated by manipulating the Pt loading. To isolate the effects of catalyst loss by keeping the volume fractions of Pt and ionomer in CCL at a constant value according to Equations (1) and (2), the thickness of CCL is decreased in correspondence with the reduction of catalyst loading. The catalyst loadings employed in the simulations and their respective CCL thicknesses are listed in Table 5.

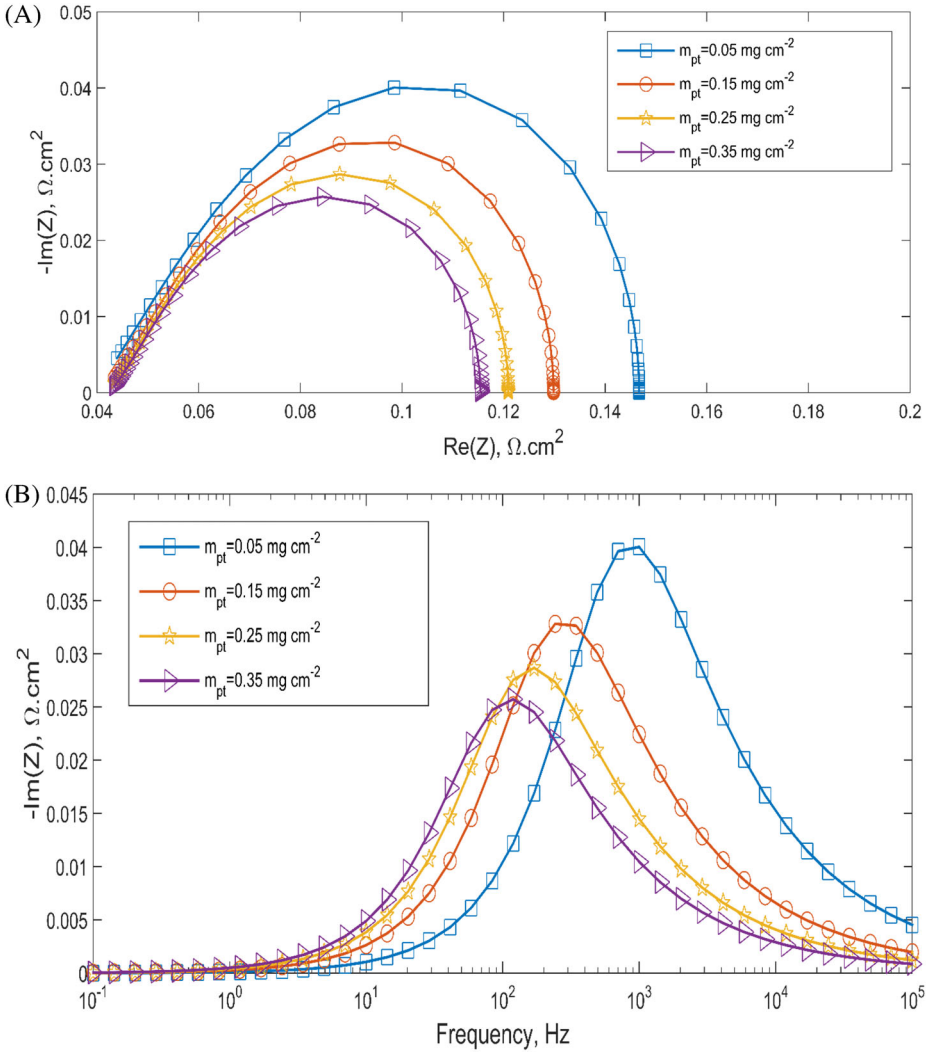


**FIGURE 11** (A) Effect of Pt loading on the impedance spectra at 1 $A/cm^2$. (B) Effect of Pt loading on the Bode plots at 1 $A/cm^2$

Figure 9 shows the effects of Pt loss on polarization curve of the cell. Decreasing Pt loading from 0.35 to 0.25 $\frac{mg}{cm^2}$ causes a small reduction in the cell output voltage due to loss of electrochemical performance. As Pt loading decreases, the rate of ORR deteriorates leading to higher activation overpotentials. As shown in Figure 10, lower ORR rate causes the liquid water saturation level in cathode, particularly in CCL, to drop due to the generation of less water as a product of ORR.

Further degradation of Pt loading from 0.25 to 0.15 $\frac{mg}{cm^2}$ leads to more pronounced changes in cell electrochemical performance. Decreasing Pt loading from 0.15 to 0.05 $\frac{mg}{cm^2}$ causes the cell performance to deteriorate drastically which highlights the importance of early identification and mitigation of Pt degradation. The experiments conducted by Xie et al[15] show similar trends of changes regarding the effect of catalyst loading on the polarization curve of the cell.

The EIS results obtained under two current densities of 1 and 1.4 $\frac{A}{cm^2}$, shown in Figures 11A and 12A, respectively, are consistent with the results of polarization curves (Figure 9) as decreasing the amount of Pt loading in CCL leads to an increase in the size of the impedance arc. The left intercept of the EIS spectrum with the real axis known as the high-frequency resistance decreases slightly as Pt loading decreases; however, the changes of the right intercept with the real axis (the low-frequency intercept) are much more pronounced (up to 27% increase in LFR under current density of 1 $\frac{A}{cm^2}$ as Pt loading decreases from 0.35 to 0.05 $\frac{mg}{cm^2}$). This makes low-frequency resistance an ideal indicator of Pt degradation in the early stages as previously stated in the literature.[33,34] Figures 11B and 12B show Bode diagrams of the cell at various Pt loadings. The frequency of the point with the largest imaginary component in the Nyquist and Bode plots is called the characteristic frequency. As the CCL becomes thinner, the characteristic frequency of the cell shifts toward lower frequencies. This could be used as an indicator of electrode losing thickness due to degradation mechanisms such as carbon corrosion.

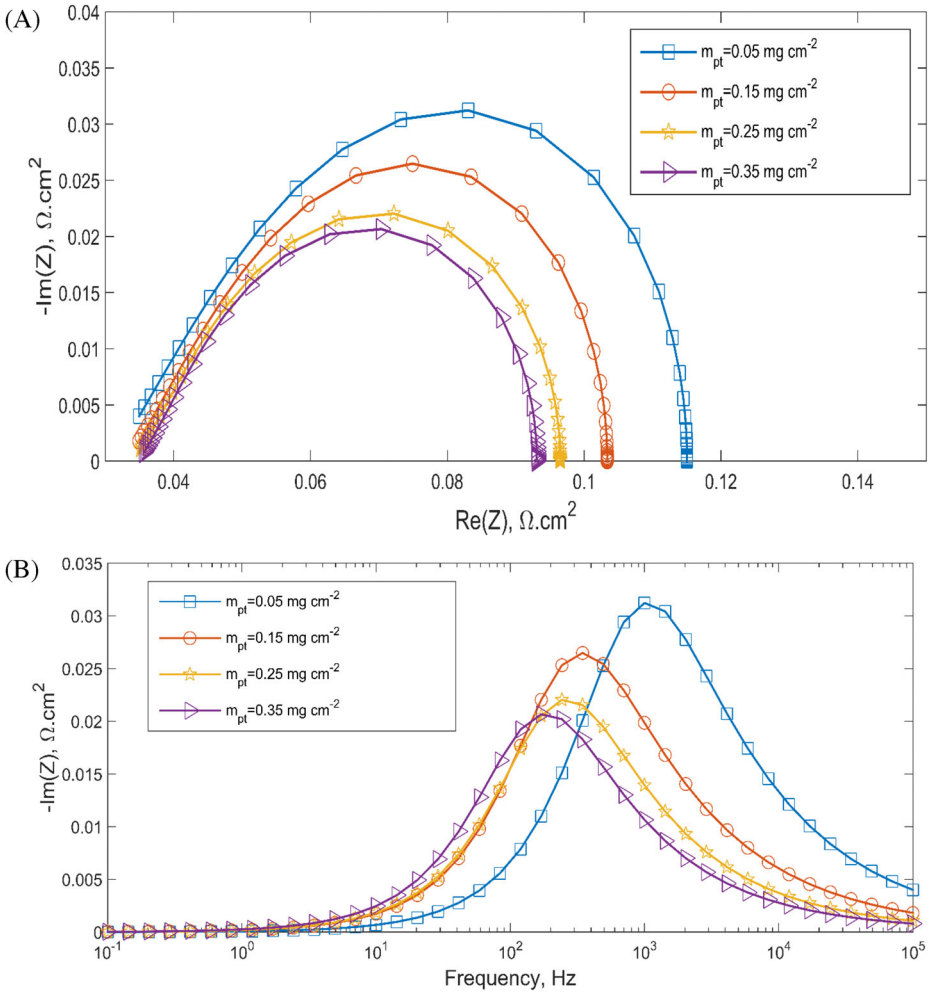


**FIGURE 12** (A) Effect of Pt loading on the impedance spectra at 1.4 $A/cm^2$. (B) Effect of Pt loading on the Bode plots at 1.4 $A/cm^2$

**TABLE 6** ionomer distributions in CCL

| | $\zeta^{0}_{im/c}$ | β | $\zeta^{avg}_{im/c}$ **(circa)** |
|---|---|---|---|
| Case 1 | 1.6 | 3.1 | 0.5 |
| Case 2 | 0.9 | 2 | 0.4 |
| Case 2 | 0.5 | 1 | 0.3 |
| Case 4 | 0.2 | 0 | 0.2 |

## 3.3 | Degradation and heterogeneous distribution of ionomer

Ionomer is an integral component of catalyst layer since it prevents cell dehydration and contributes to constructing an electrochemical reaction site for the ORR. High ionomer to carbon mass ratios are of vital importance for cells operating under low RH conditions to avert voltage drops due to high proton transfer resistance. Generation of free radicals and carbon corrosion can cause redistribution and chemical degradation of ionomer leading to loss of ionomer in CCL. In this study, to simulate the effects of ionomer degradation on PEMFC performance, four cases of heterogeneous ionomer distribution in CCL were investigated. This phenomenon is attributable to the nonuniform degradation of ionomer or the manufacturing process of the catalyst layer. The values of β and $\zeta^{0}_{im/c}$ from Equation (9) are listed in Table 6 for the cases investigated. The corresponding profiles of $\zeta_{im/c}$ in CCL are depicted Figure 13.

Figure 14 shows polarization curves of the cell for the ionomer distribution cases of Table 6. Because at higher I/C ratios, the active surface area of CCL is almost fully covered with ionomer, reduction of the I/C ratio from case 1 to case 2 causes small changes in the cell performance. As the I/C ratio is further reduced, the changes in cell performance become more pronounced to point that decreasing the I/C ratio from case 3 to case 4 causes significant performance losses since inadequate amounts of ionomer lead to lower protonic conductivity and increases the charge transfer and ohmic losses. The experiments conducted by Li et al[35] show similar trends regarding the impact of ionomer distribution on polarization curve of the cell.

The impedance spectra and Bode diagrams of the four cases listed in Table 6 are depicted in Figure 15A,B. To

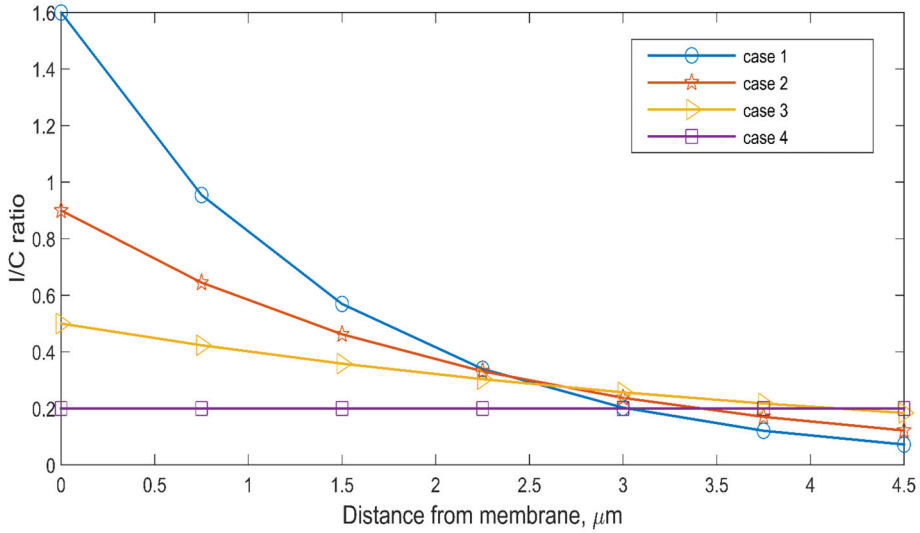


**FIGURE 13** I/C ratio profiles across the CCL for the cases from Table 6. CCL, cathode catalyst layer

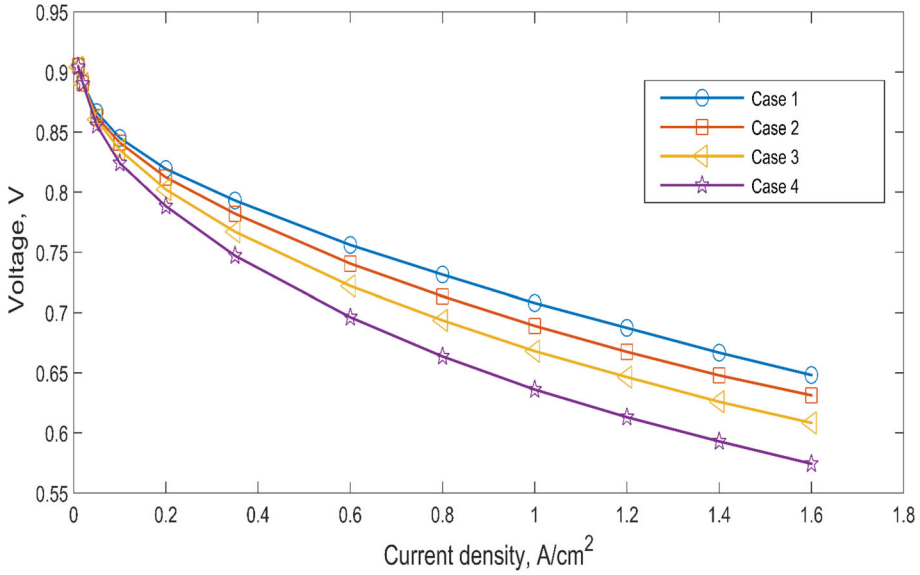


**FIGURE 14** Effect of ionomer distribution on polarization curve

mitigate the effects of water management on the high-frequency portion of the impedance spectrum, a low current density of 0.01 $^{A}/_{cm^2}$ was chosen for the EIS simulations. It is suggested in the literature,[26] that the studies regarding the effects of ionomer distribution and proton conductivity on the high-frequency portion of the impedance spectrum, should be conducted at extremely low current densities to restrain the ORR and water generation and to ensure that the changes in the impedance spectrum are solely a result of ionomer distribution and are not distorted by the effects of the cell water management. In low current densities, the impedance of the cell is dominated by kinetic losses, and hence, the effects of changing the ionomer distribution on the impedance arc are negligible. However, the high-frequency portion of the impedance spectrum shows considerable changes in correspondence with the ionomer distribution.

The expansion of the high-frequency portion of the impedance spectra of Figure 15A, referred to as the straight line in the literature, is depicted in Figure 15C. The appearance of the straight line is determined by the balance between the impacts of protonic resistance of CCL and the kinetics of ORR. If the impact of protonic resistance of CCL dominates the impact of ORR, the straight line begins to appear above a threshold value of frequency. This threshold frequency shifts toward lower values as the ionic resistance of the CCL increases. If the highest scanned frequency is larger than this threshold value, the straight line appears in the impedance spectrum. If the impact of ionic resistance of CCL is negligible compared to the impact of ORR, the high-frequency portion of the impedance spectrum will form a 90° slope with the real axis and the straight line will not take shape.

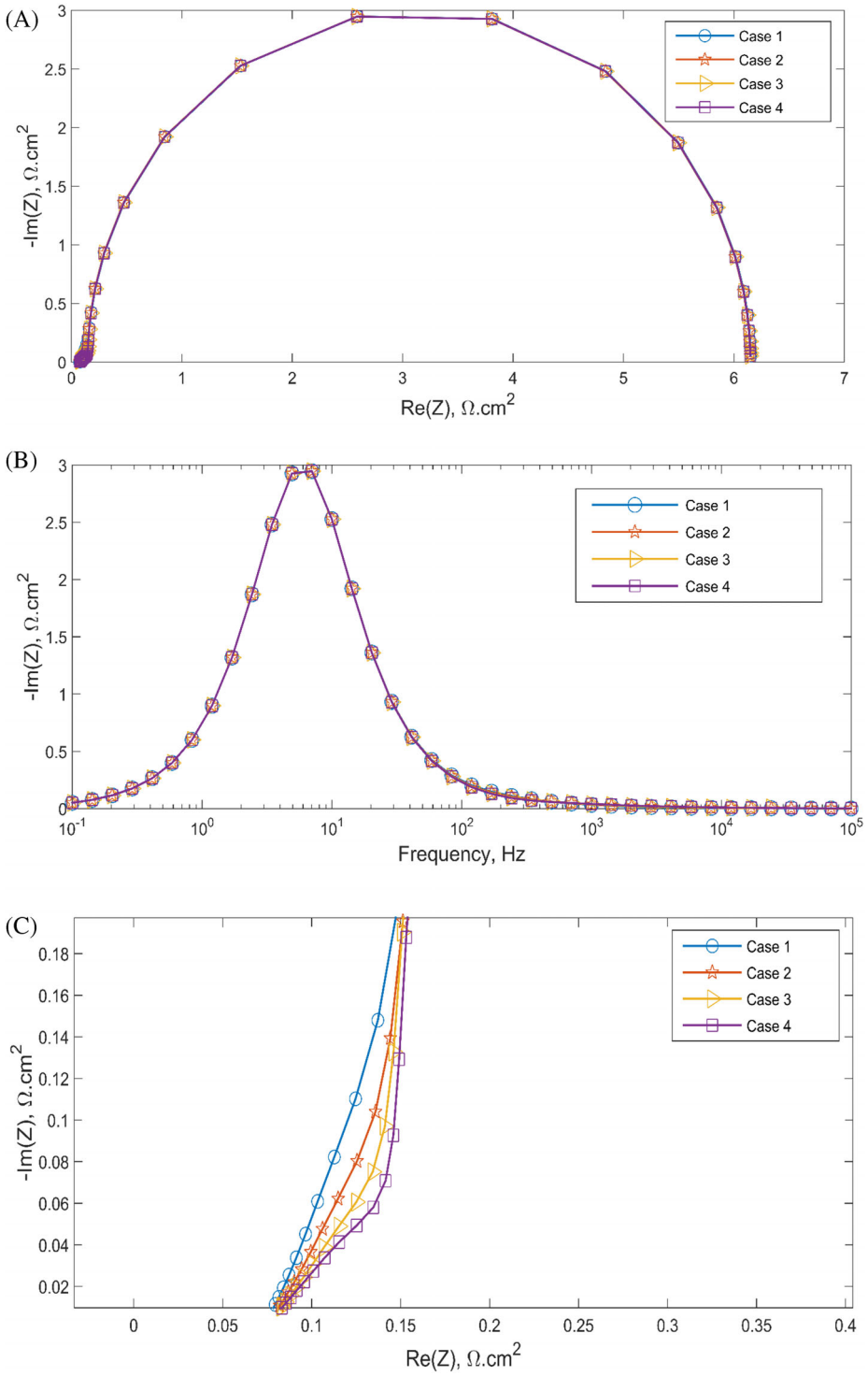


**FIGURE 15** (A) Impedance spectra at 0.01 $A/cm^2$. (B) Bode plots at 0.01 $A/cm^2$. (C) The expansion of the high-frequency portion of (A)

The slope of the straight line depends on the steepness of the $\zeta_{im/c}$ and proton conductivity gradient in CCL, hence, as the I/C ratio is reduced the slope of the straight line gradually becomes less steep. In case of a uniform distribution of the I/C ratio and proton conductivity (case 4 with $\beta = 0$), the slope of the straight line becomes the ideal 45°, however, as the $\beta$ increases to 3.1 for case 1, the slope of the straight line increases to about 61°. Reducing the I/C ratio from case 1 to case 4 also causes the length of the straight line to decrease by about 44%. The slope and length of the straight line indicate the degradation and redistribution of ionomer in CCL. Therefore, the straight line of the EIS spectra could be utilized as an effective diagnostic tool for ionomer degradation monitoring.[36]

## 4 | CONCLUSION

The aim of this study is to elucidate the interactions between CCL microstructure degradation and EIS data and to provide a reference to facilitate the interpretation of EIS data as an electrode health monitoring tool. Consequently, a computationally efficient one-dimensional, two-phase model for MEA of PEMFC with a heterogeneous distribution of ionomer in CCL was established. The balance between accuracy and computational efficiency makes this model an effective diagnostic tool for PEMFC degradation monitoring during operation. The effects of CCL microstructure degradation on cell performance were investigated and for the set of parameters and operating conditions used in the simulations, the following conclusions were achieved.

Degradation of Pt can deteriorate the kinetics of ORR, which results in higher activation losses and production of less liquid water in the cathode. The low-frequency intercept of the impedance spectrum with real axis shows the most pronounced changes with the reduction of Pt loading (up to 27% for the cases studied), therefore, is a great indicator of Pt degradation. Moreover, the characteristic frequency of the Bode diagram changes as the CCL becomes thinner which could be utilized as an indicator for degradation mechanisms such as carbon corrosion.

In case of a heterogeneous distribution of ionomer, the slope of the straight line can significantly deviate from the ideal 45° (up to 16° for the cases studied) and the length of the straight line decreases as the amount of ionomer in CCL is reduced. For the cases investigated in this study, there was a 44% reduction in the length of the straight line.

In cells operating under low RH conditions, loss of ionomer increases the cell charge transfer resistance and can significantly deteriorate cell performance. The length and the slope of the straight line at small current densities, indicate the amount of ionomer and the gradient of the ionomer distribution in CCL, respectively. Therefore, this feature of the impedance spectrum could be utilized as a tool for ionomer degradation monitoring.

## DATA AVAILABILITY STATEMENT

Data available on request due to privacy/ethical restrictions

## REFERENCES


1. Capurso T, Stefanizzi M, Torresi M, Camporeale SM. Perspective of the role of hydrogen in the 21st century energy transition. *Energ Conver Manage*. 2022;251:114898.
2. Kurnia JC, Chaedir BA, Sasmito AP, Shamim T. Progress on open cathode proton exchange membrane fuel cell: performance, designs, challenges and future directions. *Appl Energy*. 2021;283:116359.
3. Hu Z, Xu L, Gan Q, et al. Carbon corrosion induced fuel cell accelerated degradation warning: from mechanism to diagnosis. *Electrochim Acta*. 2021;389:138627.
4. Najafi B, Bonomi P, Casalegno A, Rinaldi F, Baricci A. Rapid fault diagnosis of PEM fuel cells through optimal electrochemical impedance spectroscopy tests. *Energies*. 2020;13(14):3643.
5. Sorrentino A, Sundmacher K, Vidakovic-Koch T. Polymer electrolyte fuel cell degradation mechanisms and their diagnosis by frequency response analysis methods: a review. *Energies*. 2020;13(21):5825.
6. Tang Z, Huang QA, Wang YJ, et al. Recent progress in the use of electrochemical impedance spectroscopy for the measurement, monitoring, diagnosis and optimization of proton exchange membrane fuel cell performance. *J Power Sources*. 2020;468:228361.
7. Zhang X, Zhang T, Chen H, Cao Y. A review of online electrochemical diagnostic methods of on-board proton exchange membrane fuel cells. *Appl Energy*. 2021;286:116481.
8. Ciucci F. Modeling electrochemical impedance spectroscopy. *Curr Opin Electrochem*. 2019;13:132-139.
9. Dierickx S, Weber A, Ivers-Tiffée E. How the distribution of relaxation times enhances complex equivalent circuit models for fuel cells. *Electrochim Acta*. 2020;355:136764.
10. Pan R, Yang D, Wang Y, Chen Z. Health degradation assessment of proton exchange membrane fuel cell based on an analytical equivalent circuit model. *Energy*. 2020;207:118185.
11. Touhami S, Mainka J, Dillet J, Taleb SAH, Lottin O. Transmission line impedance models considering oxygen transport limitations in polymer electrolyte membrane fuel cells. *J Electrochem Soc*. 2019;166(15):F1209-F1217.
12. Kulikovsky A. Analytical model for PEM fuel cell concentration impedance. *J Electroanal Chem*. 2021;899:115672.
13. Vivona D, Casalegno A, Baricci A. Validation of a pseudo 2D analytical model for high temperature PEM fuel cell impedance valid at typical operative conditions. *Electrochim Acta*. 2019;310:122-135.
14. Baricci A, Mereu R, Messaggi M, Zago M, Inzoli F, Casalegno A. Application of computational fluid dynamics to the analysis of geometrical features in PEM fuel cells flow fields with the aid of impedance spectroscopy. *Appl Energy*. 2017;205:670-682.
15. Xie B, Zhang G, Xuan J, Jiao K. Three-dimensional multi-phase model of PEM fuel cell coupled with improved agglomerate sub-model of catalyst layer. *Energ Conver Manage*. 2019;199:112051.
16. Falcão D, Gomes PJ, Oliveira VB, Pinho C, Pinto AM. 1D and 3D numerical simulations in PEM fuel cells. *Int J Hydrogen Energy*. 2011;36(19):12486-12498.
17. Rahman MA, Mojica F, Sarker M, Chuang PYA. Development of 1-D multiphysics PEMFC model with dry limiting current experimental validation. *Electrochim Acta*. 2019;320:134601.
18. Goshtasbi A, Pence BL, Chen J, et al. A mathematical model toward real-time monitoring of automotive PEM fuel cells. *J Electrochem Soc*. 2020;167(2):024518.
19. Esmaili Q, Nimvari ME, Jouybari NF, Chen YS. Model based water management diagnosis in polymer electrolyte membrane fuel cell. *Int J Hydrogen Energy*. 2020;45(31):15618-15629.

20. Gerteisen D. Impact of inhomogeneous catalyst layer properties on impedance spectra of polymer electrolyte membrane fuel cells. *J Electrochem Soc*. 2015;162(14):F1431-F1438.
21. Lee J, Salihi H, Lee J, Ju H. Impedance modeling for polymer electrolyte membrane fuel cells by combining the transient two-phase fuel cell and equivalent electric circuit models. *Energy*. 2022;239:122294.
22. Ren P, Pei P, Li Y, Wu Z, Chen D, Huang S. Degradation mechanisms of proton exchange membrane fuel cell under typical automotive operating conditions. *Prog Energy Combust Sci*. 2020;80:100859.
23. Wu K, Wang Z, Zhang G, et al. Correlating electrochemical active surface area with humidity and its application in proton exchange membrane fuel cell modeling. *Energ Conver Manage*. 2022;251:114982.
24. Liu J, Yin Y, Zhang J, Zhang T, Zhang X, Chen H. Mechanical degradation of catalyst layer under accelerated relative humidity cycling in a polymer electrolyte membrane fuel cell. *J Power Sources*. 2021;512:230487.
25. Gallart, M.S.. Computational modeling and optimization of proton exchange membrane fuel cells. Vol. 69. 2007.
26. Kosakian A, Secanell M. Estimating charge-transport properties of fuel-cell and electrolyzer catalyst layers via electrochemical impedance spectroscopy. *Electrochim Acta*. 2021;367:137521.
27. Lin G, He W, Van Nguyen T. Modeling liquid water effects in the gas diffusion and catalyst layers of the cathode of a PEM fuel cell. *J Electrochem Soc*. 2004;151(12):A1999.
28. Kosakian A, Urbina LP, Heaman A, Secanell M. Understanding single-phase water-management signatures in fuel-cell impedance spectra: a numerical study. *Electrochim Acta*. 2020;350:136204.
29. Bevilacqua N, Schmid M, Zeis R. Understanding the role of the anode on the polarization losses in high-temperature polymer electrolyte membrane fuel cells using the distribution of relaxation times analysis. *J Power Sources*. 2020;471:228469.
30. Narayanan H, Basu S. Development of simple diagnostic tool for proton exchange membrane fuel cell using reference electrodes in sub cells in series. *Int J Hydrogen Energy*. 2016;41(18):7659-7665.
31. Reshetenko T, Kulikovsky A. Impedance spectroscopy study of the PEM fuel cell cathode with nonuniform nafion loading. *J Electrochem Soc*. 2017;164(11):E3016-E3021.
32. Pedersen AW, Pauric AD, Eastcott JI, Easton EB. Proton conductivity within fuel cell electrodes containing a sulfonated carbon support. *ECS Trans*. 2010;28(27):39-49.
33. Pivac I, Bezmalinović D, Barbir F. Catalyst degradation diagnostics of proton exchange membrane fuel cells using electrochemical impedance spectroscopy. *Int J Hydrogen Energy*. 2018;43(29):13512-13520.
34. Meng K, Zhou H, Chen B, Tu Z. Dynamic current cycles effect on the degradation characteristic of a H2/O2 proton exchange membrane fuel cell. *Energy*. 2021;224:120168.
35. Li G, Pickup PG. Ionic conductivity of PEMFC electrodes: effect of Nafion loading. *J Electrochem Soc*. 2003;150(11):C745.
36. Gaumont T, Maranzana G, Lottin O, et al. Measurement of protonic resistance of catalyst layers as a tool for degradation monitoring. *Int J Hydrogen Energy*. 2017;42(3):1800-1812.

**How to cite this article:** Heidari H, Esmaili Q, Ranjbar AA. Model-based diagnosis of proton-exchange membrane fuel cell cathode catalyst layer microstructure degradation. *Int J Energy Res*. 2022;46(15):24408-24423. doi:10.1002/er.8755